Received: 25 September 2023 | Revised: 19 January 2024 | Accepted: 15 February 2024

DOI: 10.1002/ese3.1724

ORIGINAL ARTICLE

# The influence of methylammonium iodide concentration on the properties of perovskite solar cells

**Naveen Kumar Elangovan**[1] | **Raju Kannadasan**[1] | **Max F. Savio**[2] | **S. Vinson Joshua**[3] | **Muhammad Faheem**[4]

[1]Department of Electrical and Electronics Engineering, Sri Venkateswara College of Engineering, Chennai, India

[2]Department of Electrical and Electronics Engineering, Saveetha Engineering College, Chennai, Tamil Nadu, India

[3]Department of Electronics and Communication Engineering, Vel Tech Rangarajan Dr. Sagunthala R & D Institute of Science and Technology, Chennai, India

[4]Department of Computing Science, School of Technology and Innovations, University of Vaasa, Vaasa, Finland

**Correspondence**
Muhammad Faheem, Department of Computing Science, School of Technology and Innovations, University of Vaasa, Vaasa 65200, Finland.
Email: muhammad.faheem@uwasa.fi

**Abstract**

This study focuses on improving the quality of $MAPbI_3$-based perovskite films by adjusting the concentration ratios of the methylammonium iodide (MAI) precursor using a two-step sequential deposition method. The primary objective is to explore how altering the MAI concentration influences the microstrain, dislocation density, perovskite film quality, and their subsequent impact on the performance of perovskite solar cells. The examined device configuration $CdS/MAPbI_3$/Spiro-OMeTAD demonstrates impressive power conversion efficiency of 12.05%, $V_{oc}$ of 1.02 V, $J_{sc}$ of 16.2 mA $cm^{-2}$, and fill factor of 0.73. X-ray diffraction and scanning electron microscope analyses show improved crystal quality and surface characteristics with reduced microstrain, dislocation density, larger crystal grains, and minimized pinholes. The investigation of $MAPbI_3$'s optical and electrical characteristics provides in-depth insights, facilitating the optimization of MAI precursor concentrations for improved perovskite film development and enhanced solar cell performance.

**KEYWORDS**

dislocation density, $MAPbI_3$, microstrain, perovskite deposition, perovskite solar cell, series resistance

## 1 | INTRODUCTION

Organic–inorganic halide perovskite solar cells have garnered substantial attention due to their remarkable increase in power conversion efficiency (PCE), soaring from 3.81% to an impressive 25.7%.[1] This significant progress has positioned them as one of the most promising photovoltaic (PV) technologies. Their exceptional optical and electrical properties contribute to their appeal, boasting a large absorption coefficient of 105 $cm^{-1}$, high charge carrier mobility, and a long diffusion length ranging from 100 to 1000 nm. Additionally, these perovskite solar cells exhibit a low exciton binding energy, tunable band gap, bipolar transport

**Abbreviations:** AFM, atomic force microscopy; ETL, electron transport layer; FF, fill factor; HTL, hole transport layer; $J_{SC}$, short circuit current; PCE, power conversion efficiency; PSC, perovskite solar cells; PV, photovoltaic; $R_s$, series resistance; $R_{sh}$, shunt resistance; SEM, scanning electron microscope; $V_{OC}$, open circuit voltage; XRD, X-ray diffraction.

nature, and simplified manufacturing process.[2] Researchers have extensively explored the utilization of diverse perovskite materials—including $MAPbI_3$, $MAPbBr_3$, $MASnI_3$, $CsPbBr_3$, and $FAPbI_3$—as active layers in perovskite solar cells (PSCs).[3,4] Indeed, the quality of the perovskite material holds a substantial influence on the device's performance. Superior perovskite materials are crucial for maximizing light absorption, reducing charge recombination, and extending carrier diffusion length, all of which improve solar cell efficiency.

Undoubtedly, enhancing the quality of perovskite material stands as a key approach to boosting the performance of perovskite solar cells (PSCs). Crucial to achieving high film quality with improved crystallinity, larger grains, and smooth surfaces is the meticulous control of perovskite growth on diverse substrates.[5–7] Solution-processing techniques are predominantly used in preparing perovskite solar cells, making the composition of the precursor solution equally critical. Several solution-processing deposition methods are employed in perovskite fabrication one-step, two-step, sequential vapor deposition, two sources vapor deposition, and vapor-assisted solution deposition. Among various deposition techniques, two-step deposition method is preferred in perovskite fabrication due to several advantages over other deposition techniques: cost-effective, controlled nucleation, reduced defects, improved crystallinity, tunable properties, and enhanced stability. The electronic structure of $MAPbI_3$ exhibits high stoichiometric and surface defect tolerance factors during fabrication, rendering it insensitive to a wide range of compositional changes. However, the ideal quantity of methylammonium iodide (MAI) or $PbI_2$ precursor solution for optimal perovskite material performance remains uncertain. Additionally, researchers have proposed various mechanisms responsible for the notable enhancements observed.[8–11] It is imperative to further explore these mechanisms to gain deeper insights into the improvement of perovskite materials and, consequently, PSC efficiency.

The precursor solution's concentration ratio plays a vital role in governing the crystallinity, morphology, and colloidal properties of perovskite materials. The existing colloidal particles act as nucleation sites during the formation of perovskite films from the precursors, thereby influencing the overall film quality.[12] Hong et al. conducted a study where they carefully adjusted the MAI and $PbI_2$ ratios under Pb-rich/I-rich conditions to create $MAPbI_3$ films. They found that solvent engineering and stoichiometric ratios had a significant impact on the efficiency, photostability, surface morphology, and coverage of $MAPbI_3$ films.[13] In another approach, the addition of excess MAI to the precursor solution, combined with deposition using a Lewis acid–base adduct, effectively suppressed recombination at grain boundaries, leading to improved performance.[14] Chen et al. demonstrated that releasing organic species during the annealing process allowed the presence of the $PbI_2$ phase in the grain boundaries of perovskite, resulting in enhanced carrier behavior and stability.[15] Huang et al. found that using DMF as a solvent for MAI and $PbI_2$ was advantageous, as it controlled the crystallization rate, facilitating the formation of compact perovskite films.[16] Wieghold et al. affirmed that higher precursor concentrations contributed to the formation of larger and more oriented grains in $MAPbI_3$ films.[17] Byung-Wook Park et al. showcased how the presence of excess lead iodide in the perovskite precursor solution played a crucial role in achieving PCEs exceeding 20% by reducing halide vacancies.[18] Also, A mechanism elucidating the generation of distinct morphologies was postulated through the integration of in situ crystal growth analysis with X-ray diffraction (XRD) measurements. The thin film crystals produced at both low (60°C) and high (120°C) temperatures exhibit (110) and (200) orientations, respectively. This discrepant manner of crystal growth engenders substantially dissimilar film morphologies. In comparison to the spin-coating method, drop-casting demonstrates significantly heightened resilience against humidity-induced effects. Notably, PV cells based on $MAPbI_3$ fabricated under 88% humidity conditions yielded an impressive PCE of 18.17%. This achievement stands as the pinnacle PCE for perovskite solar cells manufactured in environments exceeding 70% humidity, all achieved without the utilization of antisolvent agents.[19]

Furthermore, many findings have been reported on the approach of various precursor concentrations using a two-step sequential deposition technique in which $PbI_2$ is coated first and MAI is spin-coated later. However, most previous studies focused on improving perovskite film quality by focusing on the process of film formation via deposition methods and tuning the concentration ratios.[20–23] Nevertheless, no detailed studies on the effect of microstrain and dislocation density on the $MAPbI_3$ perovskite film quality have been reported.

This article focuses on enhancing the quality of $MAPbI_3$-based perovskite by varying the MAI precursor concentration ratios through a sequential deposition process using the spin coating method. The investigation delves into the impact of different MAI precursor concentration ratios on the film quality of the perovskite, specifically examining microstrain and dislocation density. Extensive analysis of the $MAPbI_3$-based perovskite material and the influence of lead iodide ($PbI_2$) concentration on its properties is conducted. XRD measurements demonstrate that the perovskite film

quality experiences improvement, attaining the lowest microstrain and dislocation density with an optimal MAI (35 mg) $PbI_2$ (464 mg) precursor solution ratio. Scanning electron microscopy (SEM) reveals that the perovskite film with an optimal MAI (35 mg) ratio exhibits a larger grain size, reduced pinholes, and uniform surface coverage. The corresponding perovskite solar cell, with a device structure of FTO/CdS/MAI (35 mg) $PbI_2$/Sprio-OMeTAD/Ag, achieves an impressive PCE of 12.05%. Additionally, the study delves into the intricate properties of the perovskite material, providing valuable insights for potential future development paths. By elucidating the optimal MAI precursor concentration ratio and its influence on film quality and solar cell performance, this research paves the way for further advancements in the field of perovskite-based solar cells. Here is a summary of the contribution's points for this article:

- Enhance the quality of $MAPbI_3$-based perovskite by varying the concentration ratios of the MAI precursor using a sequential deposition technique with spin coating.
- The impact of different MAI precursor concentration ratios on film quality is investigated, focusing on microstrain and dislocation density in the perovskite material.
- XRD measurements reveal that an optimal MAI (35 mg) $PbI_2$ (464 mg) precursor solution ratio results in improved perovskite film quality with the lowest microstrain and dislocation density.
- The study also demonstrates that the perovskite film with the optimal MAI (35 mg) ratio exhibits larger grain size, reduced pinholes, and uniform surface coverage, leading to a perovskite solar cell with an impressive PCE of 12.05%.

The remaining sections of the article are organized as follows: Section 2 discusses the experimental method. Section 3 presents the fabrication and characterization. Section 4 presents the simulated results obtained from implementing the proposed methodology. Finally, Section 5 concludes the work based on the attained outcomes from the entire study.

## 2 | EXPERIMENTAL METHOD

### 2.1 | Materials

The following materials were used to prepare the material layers: MAI, methylammonium lead iodide ($MAPbI_3$), isopropyl alcohol (IPA), lead iodide ($PbI_2$), dimethyl sulfoxide (DMSO), *N*, *N*-dimethylformamide (DMF), fluorine-doped tin oxide (FTO), cadmium chloride ($CdCl_2$), liquid ammonia ($NH_3$), thiourea ($CS(NH_2)_2$), chlorobenzene, ethanol and 2,2′,7,7′-tetrakis-(*N*, *N*-di-4-methoxyphenylamino)-9,9′-spirobifluorene (Spiro-OMeTAD). Sigma-Aldrich and Sri Hari Company India supplied all of the materials used in this fabrication.

### 2.2 | Device structure

The proposed $MAPbI_3$-based perovskite solar cell has the following stack of layers: (1) FTO/CdS/$MAI_{(15\ mg)}PbI_{2(464\ mg)}$/Sprio-OMeTAD/Ag, (2) FTO/CdS/$MAI_{(25\ mg)}PbI_{2(464\ mg)}$/Sprio-OMeTAD/Ag, (3) FTO/CdS/$MAI_{(35\ mg)}PbI_{2(464\ mg)}$/Sprio-OMeTAD/Ag. The effective shading mask area of 0.09 $cm^2$ with a well-defined aperture is fabricated using a laser cutting machine, according to the key device structure. The device's active area was 1 $cm^2$. Figure 1 illustrates the device structure and energy level diagram of PSC. The overall thickness of the perovskite solar cell for Sample 1, Sample 2, and Sample 3 is measured to be around 390 nm ± 5 nm, 490 nm ± 5 nm, and 540 nm ± 5 nm, respectively, using atomic force microscopy (AFM) analysis. These thicknesses for each layer were calculated using AFM analysis and each layer is coated separately on an FTO glass with the same deposition time and RPM as mentioned for the overall device fabrication. Notably, the series resistance of the film is taken into consideration for analyzing the performance of the solar cells.

## 3 | FABRICATION AND CHARACTERIZATION

### 3.1 | Device fabrication

The unwanted FTO glass substrate was removed with HCl and zinc powder based on the device structure. The FTO glass substrate was cleaned for 15 min each with acetone, isopropyl alcohol, and deionized water using ultrasonication. Chemical bath deposition is used to fabricate the CdS layer on the FTO glass substrate. 100 mL 0.25 M $CdCl_2$ was taken in a beaker and steered until 75°C. After reaching the desired temperature, 50 mL liquid $NH_3$ was added to the solution and steered for 25 min. The solution slowly changes from colorless to yellow after adding 2.286 g thiourea. All samples were removed from the CdS chemical bath after 10 min based on a previously reported study and rinsed in deionized water.[20] The $MAPbI_3$ layer above the ETL was fabricated using a sequential deposition method.

To prepare the $PbI_2$ precursor solution, 464 mg $PbI_2$ was added to 1 mL of (7:3) (DMF + DMSO) solution and stirred

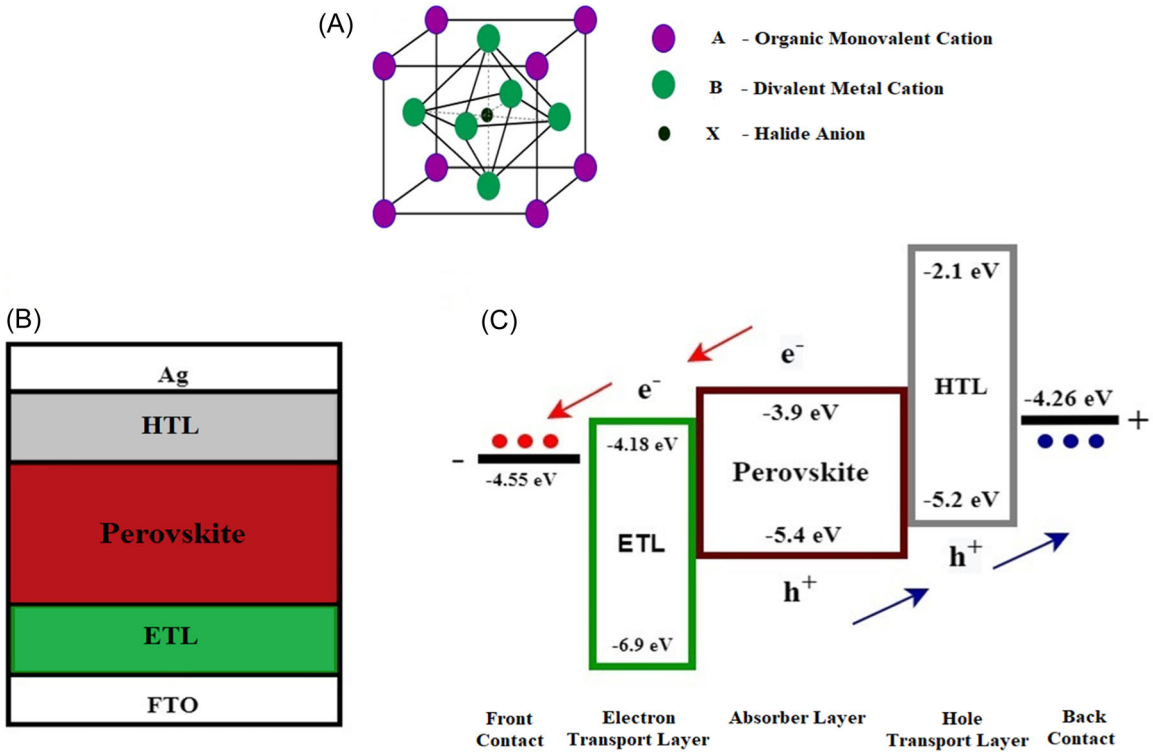


FIGURE 1 Structure and energy level diagram of perovskite solar cell (A–C).

for 2 h at 70°C. The precursor solution is then spin-coated for 30 s at 4000 rpm on the ETL before being annealed for 10 min at 100°C. Furthermore, various precursor solutions are prepared by adding 15, 25, and 35 mg of MAI to 1 mL of IPA solution and stirring continuously until the MAI is dissolved. The MAI precursor solutions are then spin-coated at 4000 rpm for 30 s above the $PbI_2$ layer of Samples 1, 2, and 3, and annealed at 70°C for 10 min. The mole percentage ratio of MAI and $PbI_2$ for Sample 1 is 8.6% and 91.4%; Sample 2 is 13.5% and 86.5%; Sample 3 is 18.1% and 81.9%, respectively. Then, 1 mL of chlorobenzene was added to 40 mg of Spiro-OMeTAD precursor solution and it is stirred continuously till the solution gets dissolved. After preparing the solution, a Spiro-OMeTAD was spin-coated over the $MAPbI_3$ layer for 20 s at 4000 rpm. To make an electrical contact above the hole transport material, Ag was sputtered. Table 1 summarizes the sequential deposition of perovskite film with various MAI precursor solution ratios. Figure 2 illustrates the two-step fabrication process of perovskite thin film.

## 3.2 | Characterization

The surface morphology of the $MAPbI_3$ layers of Samples 1, 2, and 3 was examined using a scanning electron microscope (Inspect F50-FEI). The absorption spectrum of $MAPbI_3$ samples was examined via UV-visible spectroscopy (Perkin Elmer spectrometer). The sample structure and phase identification were investigated via XRD (XPert PRO—PAN analytical), the thickness of the sample was analyzed using AFM (XE 70 Atomic Force Microscopy—Park systems), and I-V measurements were performed in the presence of AM 1.5 conditions provided by the solar simulator (Keithley Electrometer).

# 4 | RESULTS AND DISCUSSIONS

The optical properties of a $CH_3NH_3PbI_3$ film made at different MAI precursor solution ratios of Samples 1, 2, and 3 were investigated using a UV-visible spectrometer, as shown in Figure 3. According to the findings, the absorption of perovskite films increases with increasing MAI precursor ratio over the long wavelength range. The study demonstrates that the $CH_3NH_3PbI_3$ layer possessed favorable light absorption characteristics ranging around 400–700 nm for perovskite film fabricated at Sample 3. The absorption spectrum of perovskite Sample 1 and Sample 2, on the other hand, is slightly reduced. The optical bandgap energy was determined to be 1.65, 1.69, and 1.72 eV ($=1241/\lambda_{onset}$) for Samples 1, 2, and 3, respectively, which is greater than the literature reported value of 1.55 eV. However, depending on the halide

**TABLE 1** Summarization of two-step perovskite films with varying MAI precursor ratios.

| SI. No | Deposition ratio | Precursor solution preparation | | | Spin coating parameters | | Annealing temp (°C) | Annealing time | Remarks of Sample-1, Sample-2 and Sample-3 |
|---|---|---|---|---|---|---|---|---|---|
| | | Solution | Temp (°C) | Time (h) | Speed (Rpm) | Time (s) | | | |
| 1. | Sample-1 | 464 mg $PbI_2$ + DMF + DMSO | 70 | 2 | 4000 | 30 | 100 | 10 min | Perovskite peaks are observed in the XRD spectra, average crystalline size is estimated as $D = 23.88$ nm. |
| | | 15 mg MAI + IPA | Room temp | Till the solution gets dissolved | 4000 | 30 | 70 | 10 min | $PbI_2$ peaks were observed in the XRD spectra at $2\theta$ 12.7°, indicating that $PbI_2$ has not been completely converted to perovskite. Surface defects and pin holes are observed. AFM thickness = 200 nm ± 50 nm. |
| 2. | Sample-2 | 464 mg $PbI_2$ + DMF + DMSO | 70 | 2 | 4000 | 30 | 100 | 10 min | Well-defined sharp perovskite XRD peaks are observed, and the average crystalline size is estimated as $D = 24.54$ nm. |
| | | 25 mg MAI + IPA | Room temp | Till the solution gets dissolved | 4000 | 30 | 70 | 10 min | The lower intensity of the $PbI_2$ peak at $2\theta$ 12.7° was observed in the XRD spectra. Surface defects and pin holes are observed. AFM thickness = 300 nm ± 50 nm |
| 3. | Sample-3 | 464 mg $PbI_2$ + DMF + DMSO | 70 | 2 | 4000 | 30 | 100 | 10 min | Well-defined sharp perovskite XRD peaks are observed, with average crystalline size $D = 32.5$ nm. |
| | | 35 mg MAI + IPA | Room temp | Till the solution gets dissolved | 4000 | 30 | 70 | 10 min | No $PbI_2$ peak was observed in the XRD spectra. Low surface defects, fewer pinholes, and large grain sizes with smooth surfaces are observed. AFM thickness = 350 nm ± 50. |

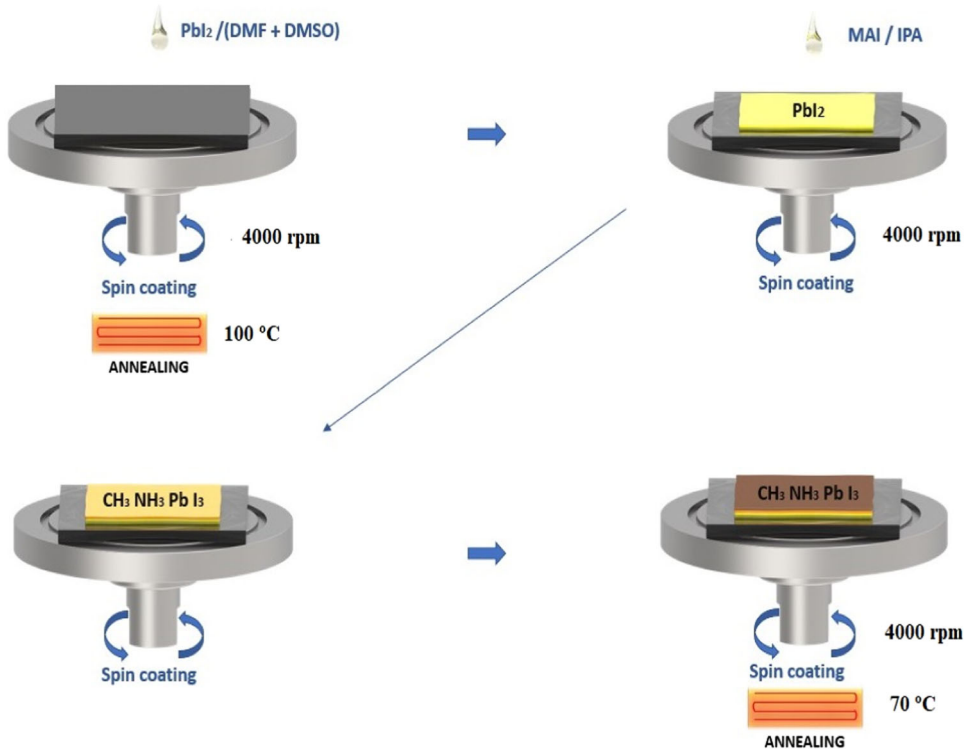


**FIGURE 2** Schematic illustration of the two-step fabrication process of perovskite film.

content and crystallite size, this energy gap is within the 1.5–2.3 eV range for halide perovskite nanomaterials.

The XRD peaks of perovskite film Samples 1, 2, and 3 are depicted in Figure 4. During the investigation of the XRD spectra of $CH_3NH_3PbI_3$, major diffraction peaks were observed for Samples 1 and 2 at 2$\theta$ 12.7°, 14.22°, 19.97°, 28.6°, 32.0°, 36.5°, and 43.2° which corresponds to (001), (110), (112), (220), (222), (241), and (314) peaks. However, $PbI_2$ peaks were observed at 2$\theta$ 12.7° which corresponds to (001) in the XRD spectra and 6.972 d-spacing, indicating that PbI2 has not been completely converted to perovskite. When compared to Sample 1, the Sample 2 film has a lower intensity of the $PbI_2$ peak. Furthermore, the presence of $PbI_2$ causes faster degradation of the $MAPbI_3$ film. Perovskite film fabricated with Sample 3 MAI precursor solution, on the other hand, appear to have major diffraction peaks at 2$\theta$ 14.22°, 19.97°, 28.6°, 32.0°, 36.5°, and 43.2° which correspond to (110), (112), (220), (222), (241), and (314) peaks of a tetragonal crystal structure. According to the data, no $PbI_2$ peaks were detected in the XRD spectra of Sample 3, indicating that $PbI_2$ has been completely converted to perovskite. On the other hand, perovskite inevitably has internal defects, such as Pb and I vacancy defects, particularly near the grain boundaries, which diminishes the stability and performance of PSC. When $MAPbI_3$-based perovskite is subjected to humid circumstances, the hydrolysis reaction weakens hydrogen bonds in the crystal lattices, degrading $PbI_2$ and changing its color from dark brown to yellow. The dominant factors causing instability are $H_2O$, $O_2$, ultraviolet light, and heat. However, the presence of excess $PbI_2$ during the fabrication of the solar cell can introduce defects or grain boundaries in the perovskite film, which can act as sites for charge recombination or promote degradation under certain conditions. Also, $PbI_2$ may contribute to the migration of ions within the perovskite layer, altering the stability of the material and leading to the degradation of the film over time.

PSCs face crucial challenges regarding stability, especially the phase instability arising from the Perovskite crystal structure and device configuration. Perovskites when used in PSC devices are subject to external factors like environmental stability, thermal stability, and photo-stability, all of which have an impact on long-term stability. The most important factor contributing to environmental stability issues in PSCs is encapsulation. Encapsulation is an effective method for extending the life of solar cells, reducing photo instability, and controlling degradation issues by acting as an oxygen and moisture barrier. Heating Perovskite beyond 100°C leads to degraded performance due to increased $PbI_2$ and organic salt formation.

The crystallite size is calculated using Debye-Scherrer's law,

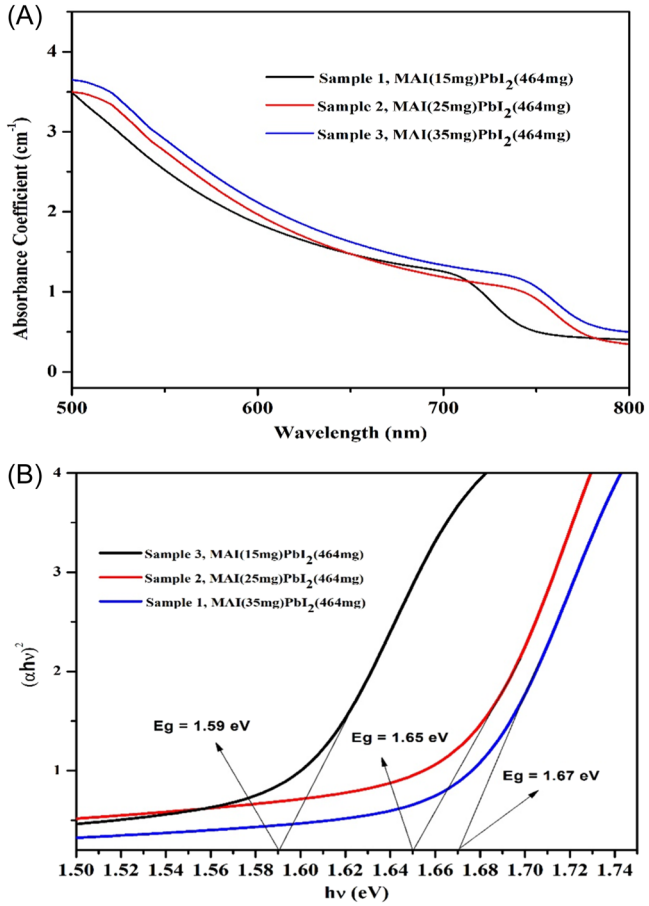


**FIGURE 3** (A) Absorption spectrum and (B) Tauc coordinates of $CH_3NH_3PbI_3$ material.

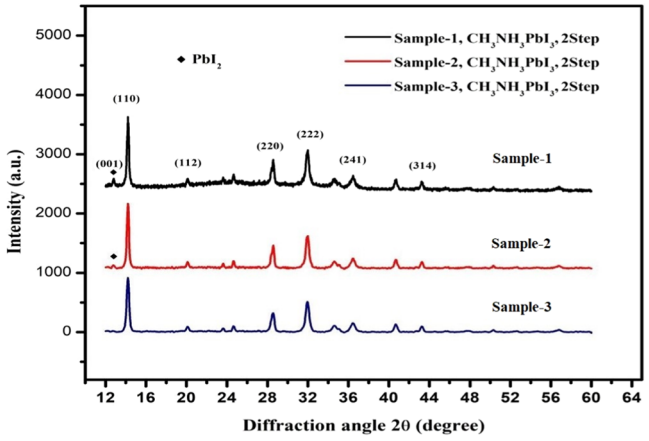


**FIGURE 4** Sample 1, 2, and 3 XRD image of $CH_3NH_3PbI_3$.

$$D = \frac{0.9\,\lambda}{\beta \cos\theta}, \tag{1}$$

where $D$ is the mean crystallite size, $\lambda$ is the wavelength of Cu, $\beta$ is the full-width half maximum (FWHM), and $\theta$ is the scattering angle. The average crystallite size of Samples 1, 2, and 3 were estimated to be 23.88, 24.54, and 32.5 nm. However, smaller crystalline sizes can introduce quantum confinement effects leading to changes in the bandgap and affecting the absorbed wavelengths (see Figure 3). Similarly, altering the halide content modifies the bandgap, enabling control over the absorption spectrum of the perovskite film for tailored opto-electronic performance.

Furthermore, the microstrain ($\varepsilon$) and dislocation density ($\delta$) were calculated from the XRD data using the following formulas,

$$\varepsilon = \frac{\beta}{4\tan\theta}, \tag{2}$$

$$\delta = \frac{n}{D^2}, \tag{3}$$

where $n$ is a factor that is nearly equal to the minimum dislocation density. The calculated values of the microstrain and dislocation density of $CH_3NH_3PbI_3$ are summarized in Table 2. Figure 5 depicts the microstrain and dislocation density of a $CH_3NH_3PbI_3$ thin film fabricated at various MAI precursor solution ratios.

The presence of the maximum microstrain is observed in the (110), (112), and (220) peaks when compared to all other peaks of perovskite. The presence of strain, according to the studies, is capable of inducing phase transitions in a crystal structure and can completely shift a material's phase diagram. Smaller microstrain, on the other hand, is usually associated with a more stable crystal. In this case, the perovskite film fabricated at 35 mg of MAI/IPA solution (Sample 3) has very low microstrain when compared to the other samples.

When related to other peaks, the dislocation density of the perovskite film is greatest for (241) and (314) peaks. The presence of dislocation density indicates that the crystal is imperfect. Furthermore, decreasing the dislocation density will increase in electron lifetime. According to the results, the film fabricated using the two-step deposition method for Sample 3 has the lowest microstrain and dislocation density. However, both the microstrain and dislocation density for the fabricated Sample 3 of perovskite film is minimal when compared to the reported literature.[24] According to the findings, the presence of maximum microstrain and dislocation density in the perovskite film may have a significant impact on the overall PV performance of the PSC while fabricating a device.[25,26]

Scanning electron microscopy is a powerful characterization technique that is used to investigate surface roughness, surface morphology, crystalline packing density, and other surface-oriented defects. Figure 6

**TABLE 2** X-ray diffraction parameters of Samples 1, 2, and 3 of $MAPbI_3$ fabricated film using a two-step deposition method.

| Samples | 2θ | Sized (nm) | d-spacing (Å) | *hkl* | $\mathcal{E}\times10^{-3}$ | $\delta\times10^{-3}$ (nm) |
|---|---|---|---|---|---|---|
| Sample 1 | 14.22 | 33.74 | 6.22 | 110 | 8.29 | 0.87 |
| | 19.97 | 24.66 | 4.44 | 112 | 8.10 | 1.64 |
| | 28.6 | 20.39 | 3.11 | 220 | 6.88 | 2.40 |
| | 32 | 19.43 | 2.79 | 222 | 6.47 | 2.64 |
| | 36.5 | 21.25 | 2.45 | 241 | 5.20 | 2.21 |
| | 43.20 | 23.85 | 2.09 | 314 | 3.94 | 1.75 |
| Sample 2 | 14.22 | 37.31 | 6.22 | 110 | 7.50 | 0.71 |
| | 19.97 | 26.02 | 4.44 | 112 | 7.68 | 1.47 |
| | 28.6 | 21.69 | 3.11 | 220 | 6.46 | 2.12 |
| | 32 | 20.73 | 2.79 | 222 | 6.06 | 2.32 |
| | 36.5 | 22.5 | 2.45 | 241 | 4.92 | 1.97 |
| | 43.20 | 18.98 | 2.09 | 314 | 4.95 | 2.77 |
| Sample 3 | 14.22 | 39.02 | 6.22 | 110 | 7.51 | 0.71 |
| | 19.97 | 35.07 | 4.44 | 112 | 5.69 | 0.81 |
| | 28.6 | 48.8 | 3.11 | 220 | 2.86 | 0.41 |
| | 32.0 | 25.04 | 2.79 | 222 | 5.02 | 1.59 |
| | 36.5 | 20.4 | 2.45 | 241 | 5.42 | 2.40 |
| | 43.2 | 26.7 | 2.09 | 314 | 3.52 | 1.40 |

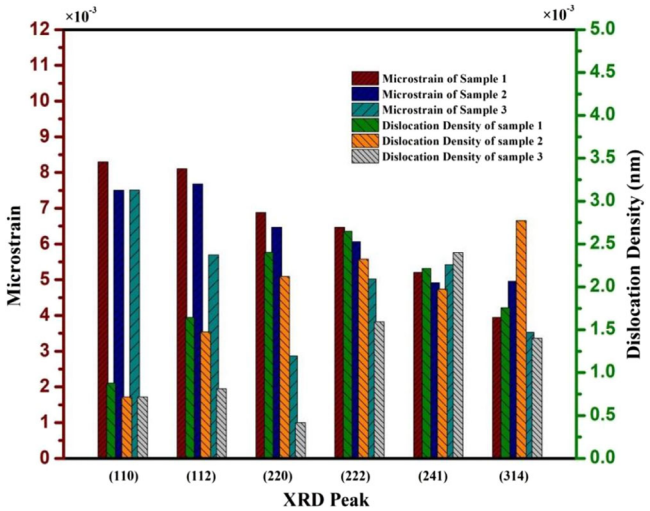


**FIGURE 5** Calculated microstrain and dislocation density of $CH_3NH_3PbI_3$ film fabricated at different MAI precursor ratios of Samples 1, 2, and 3.

shows an SEM image of a fabricated $CH_3NH_3PbI_3$ thin film. According to the results, Sample 3 film fabricated using the sequential deposition method has fewer observable pinholes, good crystalline quality, a large grain size, and uniform surface coverage, which has the potential to reduce leakage current and suppress the recombination effect when applied to solar cell applications. However, the presence of pin-holes in Samples 1 and 2 may allow direct contact of the charge transport layers through the perovskite layer, resulting in a larger hysteresis effect and lower PCE. Surface homogeneity is important in the making of a good-quality solar cell device. The final solar cell device performance will be very poor when the surface has a large number of pinholes, disorders, and uneven grain formation. The strong and efficient perovskite solar cell device architecture is based mainly on the surface quality of the perovskite film. Whereas, the presence of surface porosity will lead to an immediate recombination effect and the photo-generated carrier will recombine near the defect area. Hence the device's final output will be very poor and in some cases, the device will not work. In addition, Samples 1, 2, and 3 films are subjected to AFM analysis to determine the sample's thickness. As shown in Figure 7, the film fabricated using the two-step deposition method for Samples 1, 2, and 3 has a thickness of $200\,\text{nm} \pm 50\,\text{nm}$, $300\,\text{nm} \pm 50\,\text{nm}$, and $350\,\text{nm} \pm 50\,\text{nm}$. According to previous studies, increasing the thickness of the active layer from 100 to 1000 nm shows an increase in the photogeneration of the electron–hole pair. However, as the thickness increases beyond the diffusion length, the PCE decreases.[27–29]

The effect of various MAI precursor concentration ratios prepared using the sequential deposition method on the performance of the Perovskite solar cell was investigated.

To analyze the PV performance of a perovskite solar cell, four key solar cell parameters, namely PCE, FF, $V_{oc}$, and $J_{sc}$, are summarized in Table 3. The FF and PCE of perovskite solar cells were used to evaluate their overall performance.

$$FF = \frac{V\,\text{max} \times I\,\text{max}}{Voc \times Jsc}, \tag{4}$$

$$\eta = \frac{Voc \times Jsc \times FF}{Pin}, \tag{5}$$

where $V_{max}$ represents the maximum photovoltage, $I_{max}$ represents the maximum photocurrent, $P_{in}$ represents the incident light, and $J_{sc}$, and $V_{oc}$ represents the short-circuit current and open-circuit voltage. In this process, the device architecture of the PSC with device structure CdS/MAI(35 mg)$PbI_2$/Sprio-OMeTAD/Ag showed a very good PCE of 12.05%. According to the findings, perovskite material quality was the first major significant parameter used in determining the performance of PSCs. The series

resistance of a perovskite film fabricated for Sample 3 precursor solution ratio is $R_s = 6.28\,\Omega.cm^2$. Films made with Sample 1 and 2 precursor solutions, on the other hand, have series resistances of $R_s = 7.61$ and $7.15\,\Omega.cm^2$, respectively. Increases in the MAI precursor solution ratios had a significant impact on increasing PCE. According to the findings, increasing the MAI precursor solution ratios results in increased film thickness, improved film quality, and decreased microstrain, dislocation density, and series resistance. As a result, a thicker perovskite layer promotes the generation of electron–hole pairs.[30–33] Perovskite has a diffusion length ranging from 100 to 1000 nm, so increasing the thickness of the perovskite layer in relation to the diffusion length and overall device architecture results in improved generation of charge carriers.

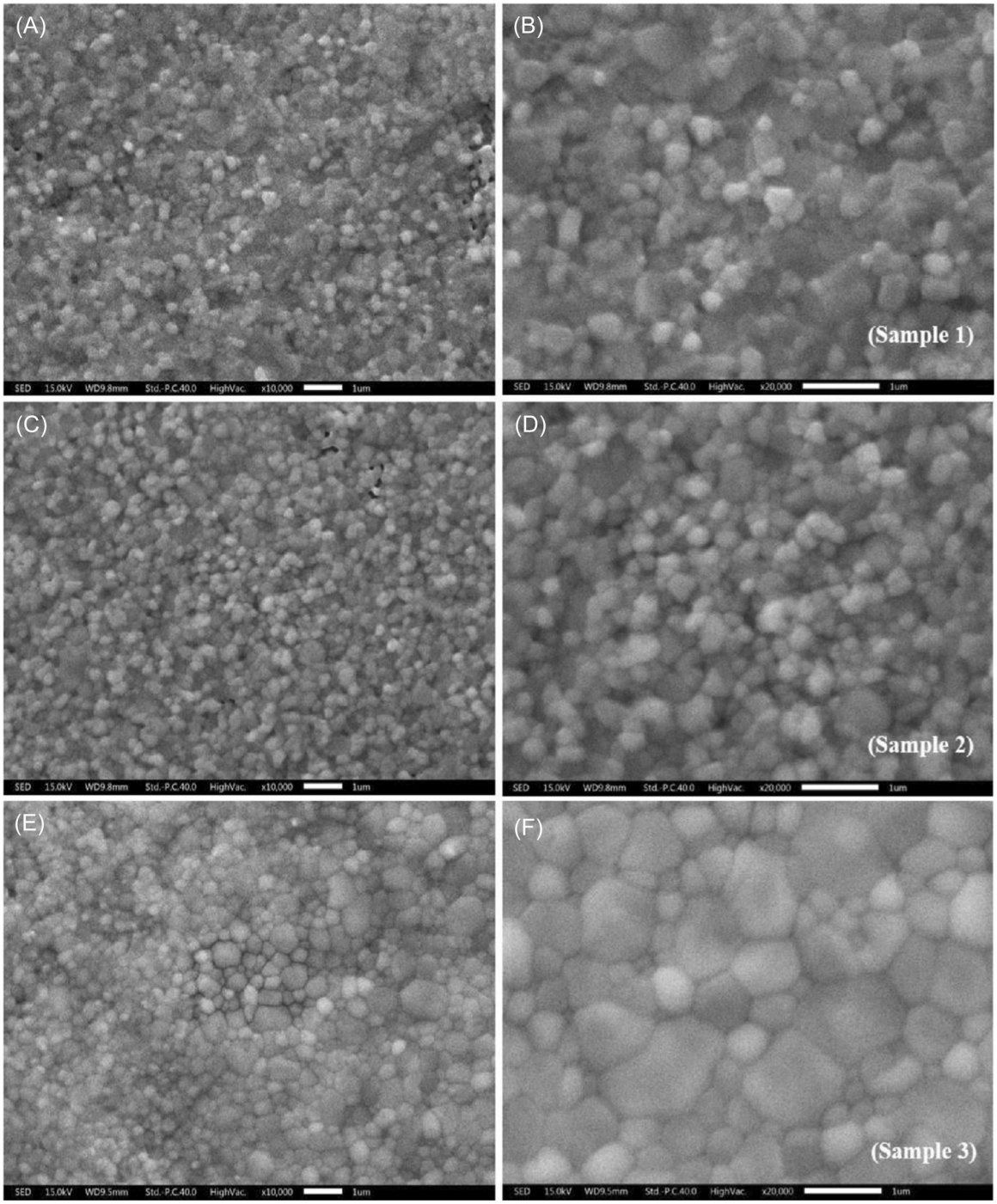


**FIGURE 6** SEM top surface morphology of the fabricated two-step perovskite (A) 1 μm ×10,000 and (B) 1 μm ×20,000 of Sample 1, (C) 1 μm ×10,000 and (D) 1 μm ×20,000 of Sample 2, (E) 1 μm ×10,000 and (F) 1 μm ×20,000 of Sample 3.

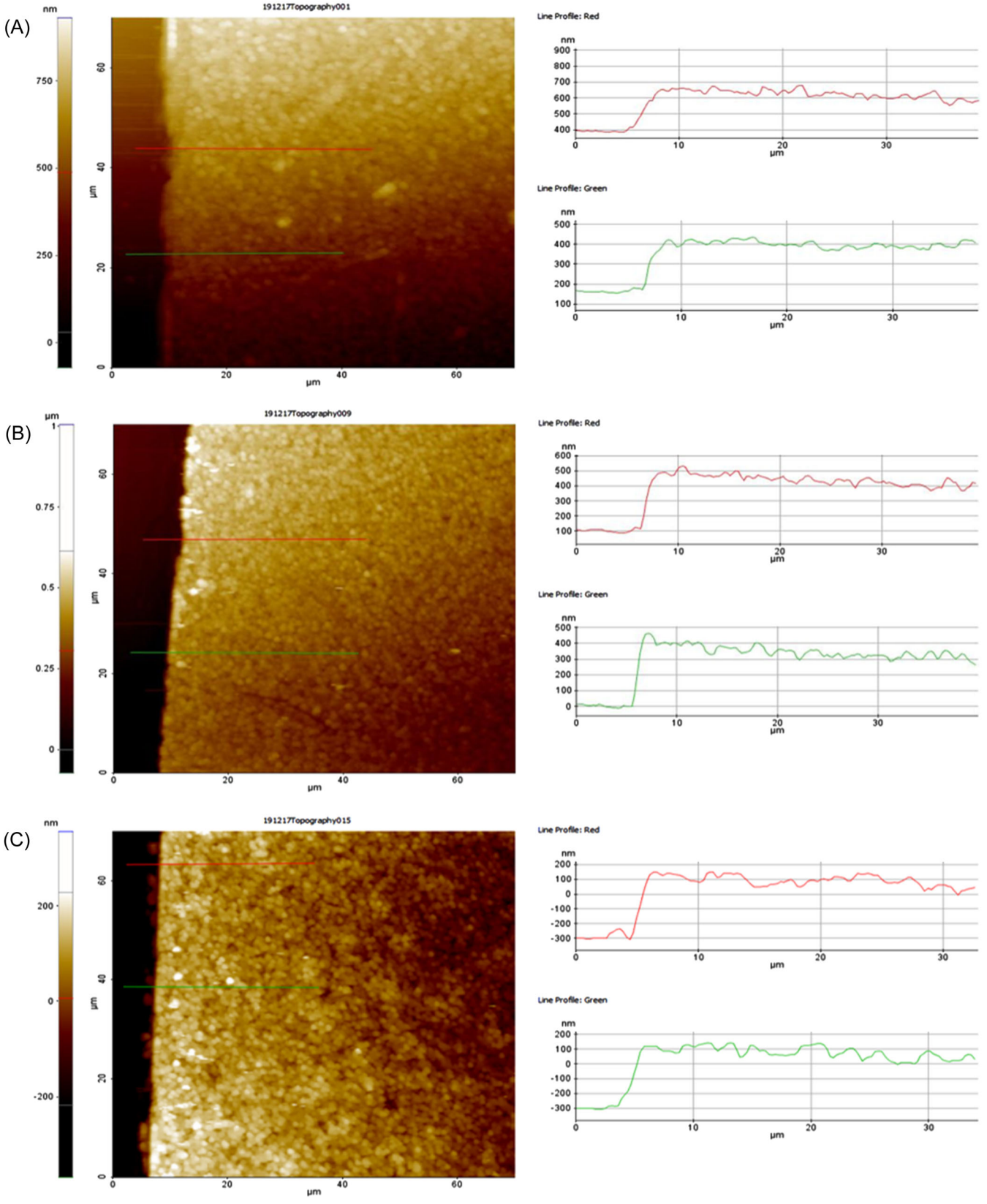


FIGURE 7 AFM image of $MAPbI_3$ thin film (A) Sample 1, (B) Sample 2, and (C) Sample 3.

TABLE 3 PV parameters for the PSC with various MAI precursor solution ratios.

| Device structure with overall device thickness | $J_{sc}$ (mA/cm$^2$) | $V_{oc}$ (V) | FF | PCE (%) | $R_{sh}$ (Ω) | $R_s$ (Ω) |
|---|---|---|---|---|---|---|
| FTO/CdS/MAI$_{(15\ mg)}$PbI$_2$/Sprio-OMeTAD (390 nm ± 5 nm) | 13.4 | 1.01 | 0.715 | 9.73 | 1737 | 7.61 |
| FTO/CdS/MAI$_{(25\ mg)}$PbI$_2$/Sprio-OMeTAD (490 nm ± 5 nm) | 14.5 | 1.01 | 0.719 | 10.60 | 1852 | 7.15 |
| FTO/CdS/MAI$_{(35\ mg)}$PbI$_2$/Sprio-OMeTAD (540 nm ± 5 nm) | 16.2 | 1.02 | 0.728 | 12.05 | 3475 | 6.28 |

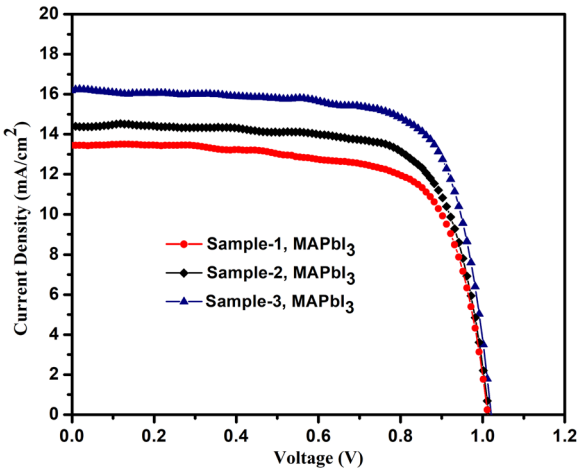


FIGURE 8 *J–V* curve of MAPbI$_3$-based PSC on various precursor solution ratios.

Based on the observations from Figure 8, it is found that the initial behavior of the solar cell shows inhomogeneous characteristics for the various MAI precursor solution ratios of PSCs; it is due to the effect of series resistance. Also, the transportation of charges from the perovskite to the electron and hole transport layers is hampered by poor film quality, resulting in increased series resistance by causing a recombination effect in the device that upholds the inhomogeneous. This recombination effect declined the generation of photocurrent and efficiency of the perovskite solar cell. However, increasing the MAI precursor solution ratios results in better perovskite film quality for increasing the voltage for all the considered samples. On the other hand, a decrease in PCE could be caused by interfacial resistance at ETL/Perovskite or Perovskite/HTL interfaces. Moreover, the use of a nano-rod or nano-wire arrangement for the electron transport layer could result in a further decrease in interfacial resistance. As a result, the study shows that increasing the MAI precursor solution ratios causes a gradual increase in perovskite solar cell performance. In contrast to voltage, the short circuit current density of the PSC changes dramatically with the various precursor solution ratios. Relating the existing work notably reported by Jeong-Hyeok Im et al.,[34] the proposed work extensively focuses on the effect of MAPbI$_3$ microstrain, dislocation density, device thickness, and series resistance that impact the overall performance of perovskite solar cells which were not considered by the existing work.

## 5 | CONCLUSIONS

According to the findings, the perovskite film fabricated using the optimal MAI precursor solution ratio of Sample 3 has no PbI$_2$ peaks and has the least amount of microstrain and dislocation density. SEM analysis, on the other hand, shows that the film fabricated using Sample 3 precursor solution ratio has fewer observable pinholes, which reduces leakage current and suppresses the recombination effect in the perovskite solar cell. The UV-visible, XRD, SEM, and AFM data from Samples 1, 2, and 3 indicate that the Sample 3 precursor solution ratio is the best for preparing MAPbI$_3$-based perovskite films using a two-step spin coating deposition method. The highest PCE of 12.05%, $V_{oc}$ of 1.02 V, $J_{sc}$ 16.2 mA cm$^{-2}$, and FF of 0.728 were obtained for an optimum MAI precursor solution ratio of Sample 3 for the following device structure CdS/MAI$_{(35\ mg)}$PbI$_{2(464\ mg)}$/Spiro-OMeTAD. These findings suggest that increasing microstrain, dislocation density, and series resistance will have a significant impact on the performance of a PSC. Furthermore, the findings of this study will provide a quantitative understanding of the working mechanism of a PSC, allowing for further performance enhancement.

## ACKNOWLEDGMENTS

The authors express their gratitude to their affiliated institutes for the financial support provided to conduct this study.

## CONFLICT OF INTEREST STATEMENT

The authors declare no conflict of interest.

## ORCID

*Raju Kannadasan* http://orcid.org/0000-0001-7622-8261
*Muhammad Faheem* http://orcid.org/0000-0003-4628-4486

## REFERENCES

1. National Renewable Energy Laboratory. *Best Research-Cell Efficiency Chart*. 2022. www.nrel.gov/pv/cell-efficiency.html
2. Singh S, Hossain A, Maddow-Zimet I, Vlassoff M, Bhuiyan HU, Ingerick M. The incidence of menstrual regulation procedures and abortion in Bangladesh, 2014. *Int Perspect Sexual Reproduct Health*. 2017;43(1):1-11. doi:10.1363/43e2417
3. Zhao Y, Ye Q, Chu Z, Gao F, Zhang X, You J. Recent progress in high-efficiency planar-structure perovskite solar cells. *Energy Environ Mater*. 2019;2(2):93-106. doi:10.1002/eem2.12042
4. Alturisa MI, Wira J, Mardiyati M, Herman R, Hidayat R. Influences of precursor solution concentration and temperature on $CH_3NH_3PbI_3$ perovskite layer morphology and the unconverted $PbI_2$ proportion to their perovskite solar cell characteristics. *J Phys: Conf Ser*. 2017;877(1):012046. doi:10.1088/1742-6596/877/1/012046
5. Wang Y, Xu H, Wang F, et al. Unveiling the guest effect of n-butylammonium iodide towards efficient and stable 2D–3D perovskite solar cells through sequential deposition process. *Chem Eng J*. 2020;391:123589. doi:10.1016/j.cej.2019.123589
6. Kim EB, Akhtar MS, Shin HS, Ameen S, Nazeeruddin MK. A review on two-dimensional (2D) and 2D-3D multidimensional perovskite solar cells: perovskites structures, stability, and photovoltaic performances. *J Photochem Photobiol, C*. 2021;48:100405. doi:10.1016/j.jphotochemrev.2021.100405
7. Elangovan NK, Arumugam S. Chayaver: Indian-traditional dye to modern dye-sensitized solar cells. *Mater Res Express*. 2019;6(6):066206. doi:10.1088/2053-1591/ab0cad
8. Bahtiar A, Rahmanita S, Inayatie YD. Pin-hole free perovskite film for solar cells application prepared by controlled two-step spin-coating method. *IOP Conf Ser Mater Sci Eng*. 2017;196(1):012037. doi:10.1088/1757-899X/196/1/012037
9. Ozaki M, Shimazaki A, Jung M, et al. A purified, solvent-intercalated precursor complex for wide-process-window fabrication of efficient perovskite solar cells and modules. *Angew Chem Int Ed*. 2019;58(28):9389-9393. doi:10.1002/anie.201902235
10. Chen LC, Lee KL, Wu WT, et al. Effect of different $CH_3NH_3PbI_3$ morphologies on photovoltaic properties of perovskite solar cells. *Nanoscale Res Lett*. 2018;13:140. doi:10.1186/s11671-018-2556-8
11. Zhang ZL, Men BQ, Liu YF, Gao HP, Mao YL. Effects of precursor solution composition on the performance and I–V hysteresis of perovskite solar cells based on $CH_3NH_3PbI_{3-x}Cl_x$. *Nanoscale Res Lett*. 2017;12(1):84. doi:10.1186/s11671-017-1872-8
12. Jiang S, Sheng Y, Hu Y, Rong Y, Mei A, Han H. Influence of precursor concentration on printable mesoscopic perovskite solar cells. *Front Optoelectron*. 2020;13(3):256-264. doi:10.1007/s12200-020-1013-3
13. Hong D, Xie M, Tian Y. Photostable and uniform $CH_3NH_3PBI_3$ perovskite film prepared via stoichiometric modification and solvent engineering. *Nanomaterials*. 2021;11(2):405. doi:10.3390/nano11020405
14. Son DY, Lee JW, Choi YJ, et al. Self-formed grain boundary healing layer for highly efficient $CH_3NH_3PbI_3$ perovskite solar cells. *Nat Energy*. 2016;1(7):16081. doi:10.1038/nenergy.2016.81
15. Chen Q, Zhou H, Song TB, et al. Controllable self-induced passivation of hybrid lead iodide perovskites toward high performance solar cells. *Nano Lett*. 2014;14(7):4158-4163. doi:10.1021/nl501838y
16. Chen D, Dong H, Pang S, et al. Enhancing material quality and device performance of perovskite solar cells via a facile regrowth way assisted by the DMF/chlorobenzene mixed solution. *Org Electron*. 2019;70:300-305. doi:10.1016/j.orgel.2019.04.012
17. Wieghold S, Correa-Baena JP, Nienhaus L, et al. Precursor concentration affects grain size, crystal orientation, and local performance in mixed-ion lead perovskite solar cells. *ACS Appl Energy Mater*. 2018;1(12):6801-6808. doi:10.1021/acsaem.8b00913
18. Park B, Kedem N, Kulbak M, et al. Understanding how excess lead iodide precursor improves halide perovskite solar cell performance. *Nat Commun*. 2018;9(1):3301. doi:10.1038/s41467-018-05583-w
19. Zuo C, Ding L. Drop-casting to make efficient perovskite solar cells under high humidity. *Angew Chem Int Ed*. 2021;60:11242-11246.
20. Sivaprakasam A, Elangovan NK. Effect of CdS thin film on the performance of methylammonium lead iodide perovskite solar cell. *J Mater Sci: Mater Electron*. 2021;32(13):17612-17619. doi:10.1007/s10854-021-06294-7
21. Abulikemu M, Barbé J, El A, et al. Planar heterojunction perovskite solar cell based on CdS electron transport layer. *Thin Solid Films*. 2017;636:512-518.
22. Haque F, Wright M, Mahmud MA, et al. Effects of hydroiodic acid concentration on the properties of $CsPbI_3$ perovskite solar cells. *ACS Omega*. 2018;3(9):11937-11944. doi:10.1021/acsomega.8b01589
23. El-Naggar AM, Mohamed MB, Osman MM, et al. Optical and structure properties of $CH_3NH_3PbI_3$ perovskite films doped with cesium. *Eur Phys J Appl Phys*. 2021;96:10302. doi:10.1051/epjap/2021210160
24. Wu J, Liu SC, Li Z, et al. Strain in perovskite solar cells: origins, impacts and regulation. *Natl Sci Rev*. 2021;8(8):1-8. doi:10.1093/nsr/nwab047
25. Elangovan NK, Sivaprakasam A. Investigation of parameters affecting the performance of perovskite solar cells. *Mol Cryst Liq Cryst*. 2020;710(1):66-73. doi:10.1080/15421406.2020.1829425
26. Iakobson OD, Gribkova OL, Tameev AR, Nunzi JM. A common optical approach to thickness optimization in polymer and perovskite solar cells. *Sci Rep*. 2021;11(1):5005. doi:10.1038/s41598-021-84452-x
27. Sławek A, Starowicz Z, Lipiński M. The influence of the thickness of compact $TiO_2$ electron transport layer on the performance of planar $CH_3NH_3PBI_3$ perovskite solar cells. *Materials*. 2021;14(12):3295. doi:10.3390/ma14123295

28. Min Nam Y, Huh J, Ho Jo W. Optimization of thickness and morphology of active layer for high performance of bulk-heterojunction organic solar cells. *Sol Energy Mater Sol Cells*. 2010;94(6):1118-1124. doi:10.1016/j.solmat.2010.02.041
29. Hasan I, Joshi S, Subbaya KM, Elangovan NK. Developments in perovskite materials based solar cells: in pursuit of hysteresis effect, stability issues and lead-free based perovskite materials. *Nanosci Nanotechnol-Asia*. 2022;12(3):46-61. doi:10.2174/2210681212666220718125121
30. Mariyappan P, Chowdhury TH, Subashchandran S, Bedja I, Ghaithan HM, Islam A. Influence of inorganic $NiO_x$ hole transport layer on the growth of $CsBi_3I_{10}$ perovskite films for photovoltaic applications. *Adv Mater Interfaces*. 2021;8:1-9. doi:10.1002/admi.202002083
31. Inamul Hasan Z, Joshi S, Subbaya KM. Halide-based $CH_3NH_3PbI_3$ hybrid perovskite thin films structural studies using synchrotron source X-ray diffraction. *J Mater Sci: Mater Electron*. 2022;33(20):16369-16382. doi:10.1007/s10854-022-08528-8
32. Lekesi LP, Koao LF, Motloung SV, Motaung TE, Malevu T. Developments on perovskite solar cells (PSCs): a critical review. *Applied Sciences*. 2022;12(2):672. doi:10.3390/app12020672
33. Hasan ZI, Joshi S, K. M. S, Parameshwara S. Surface interface structural studies of $CH_3NH_3PbI_3$ thin films using synchrotron source X-ray diffraction for solar cell application. *Mater Today: Proc*. 2022;64:1837-1843. doi:10.1016/j.matpr.2022.06.185
34. Bouich A, Torres JC, Chfii H, et al. Delafossite as hole transport layer a new pathway for efficient perovskite-based solar sells: insight from experimental, DFT and numerical analysis. *Sol Energy*. 2023;250:18-32. doi:10.1016/j.solener.2022.12.022

**How to cite this article:** Elangovan NK, Kannadasan R, Savio MF, Vinson Joshua S, Faheem M. The influence of methylammonium iodide concentration on the properties of perovskite solar cells. *Energy Sci Eng*. 2024;12:2004-2016. doi:10.1002/ese3.1724